

Pb_{1-x}Ca_xTiO₃ solid solution (x=0.0, 0.25, 0.50, and 0.75): A theoretical and experimental approach

Sérgio Ricardo de Lázaro*

Departamento de Química, Universidade Federal de São Carlos, Caixa Postal 676, 13565-905 São Carlos, SP, Brazil

Poty Rodrigues de Lucena

Instituto de Ciências Ambientais e Desenvolvimento Sustentável, Universidade Federal da Bahia, Barreiras, Ba, Brazil

Júlio Ricardo Sambrano

Laboratório de Simulação Molecular, DM, Universidade Estadual Paulista, Caixa Postal 473, 17033-360, Bauru, SP, Brazil

Paulo Sérgio Pizani

Departamento de Física, Universidade Federal de São Carlos, Caixa Postal 676, 13565-905 São Carlos, SP, Brazil

Armando Beltrán

Departament de Ciències Experimentals, Universitat Jaume I, P.O. Box 6029 AP, 12080 Castelló, Spain

José Arana Varela and Elson Longo

Instituto de Química, UNESP, P.O. Box 355, 14801-970, Araraquara, SP, Brazil

(Received 19 July 2006; revised manuscript received 13 February 2007; published 25 April 2007)

In this paper we report an experimental and theoretical study based on a periodic density functional investigation into selected compositions of Pb_{1-x}Ca_xTiO₃ (x=0.0, 0.25, 0.50, and 0.75). Based on our findings, we propose that the pseudocubic structure of these perovskites presents a long-range tendency for cubic symmetry, while the short-range displacements bring the solid solution to a tetragonal symmetry. The results are discussed in terms of x-ray diffraction, structural optimized parameters, Raman spectroscopy, band structure, density of states, Mulliken charge, and overlap population.

DOI: [10.1103/PhysRevB.75.144111](https://doi.org/10.1103/PhysRevB.75.144111)

PACS number(s): 71.15.Mb, 77.80.Bh, 61.50.Ah, 61.10.Nz

I. INTRODUCTION

ABO₃ perovskite oxides constitute an important family of ferroelectrics (FEs) whose relatively simple chemical and crystallographic structures have contributed significantly to our understanding of FE and antiferroelectric phenomena.¹ Some prototypical soft phonon mode systems in either pure or mixed crystal form readily undergo structural phase transitions involving both polar and nonpolar distortions of the cubic or tetragonal lattice.² PbTiO₃ (PT) has attracted considerable attention in recent years, because it constitutes one of the major classes of ferroelectric oxides and is an ideal ferroelectric model to study electronic properties in the light of theoretical and experimental results.^{3,4}

The off-center motions of the titanium atom in the center of a tetragonal cell in PbTiO₃ are responsible for the spontaneous polarization of ferroelectric domains by the action of a directional electric field.² In the ferroelectric tetragonal phase, the Ti atom is displaced in relation to its oxygen cage along the (001) direction.⁵ In perovskite oxides, the frequency shift of the E(1TO) soft mode can be correlated to tetragonal-cubic phase transition and the presence of forbidden Raman peaks to short-range disorder effects. On the other hand, x-ray diffraction (XRD) experiments reveal the long-range arrangement of atoms in a periodic structure.⁶ Detailed knowledge of the structure in this class of oxides is very important to elucidate the nature of their ferroelectric properties.

Ca-modified lead titanate solid solution, Pb_{1-x}Ca_xTiO₃, has received considerable attention both in thin film and bulk form due to its strong piezoelectric effects and good ferroelectric and pyroelectric properties.⁷⁻⁹ In the Pb_{1-x}Ca_xTiO₃ perovskite structure (PCT), the Pb and Ca share the vertices of the unit cell and the titanium is at the center of the structure, surrounded by six oxygen atoms that occupy the middle of the faces in a regular octahedral configuration. Some papers report that calcium doping of the PbTiO₃ structure decreases the tetragonality factor (*c/a* is the lattice parameters ratio).¹⁰ At around 40% of Ca²⁺ doping, a phase transition occurs from the tetragonal to the cubic.

In an early application of x-ray diffraction to the analysis of crystal structure, Vergard observed that many ionic salts alloy a linear relation, at constant temperature, between the crystal lattice constants and concentration.^{11,12} This law has several physical factors affecting the crystal structures can be readily identified.¹³ These include (i) the relative atomic sizes of the elements, (ii) the relative volume per valence electron in crystals of the pure elements, (iii) Brillouin-zone effects, and (iv) electrochemical differences between the elements.

Dielectric and Raman experiments performed by Pontes *et al.*¹⁴ on PCT thin films as a function of temperature show a broad ferroelectric phase and a linear dependence of the transition temperature on increasing Ca content. Recently, Chopra and co-workers¹⁵ reported that PCT is formed at 650 °C with a tetragonal structure and that the tetragonality

TABLE I. Calculated theoretical and experimental lattice parameters (\AA), tetragonality factor (c/a), and Ti, O_{axial} , and $O_{\text{equatorial}}$ atomic fractional coordinates (x, y, z) for $\text{Pb}_{1-x}\text{Ca}_x\text{TiO}_3$ solid solution.

	PbTiO_3		$\text{Pb}_{0.75}\text{Ca}_{0.25}\text{TiO}_3$		$\text{Pb}_{0.50}\text{Ca}_{0.50}\text{TiO}_3$		$\text{Pb}_{0.25}\text{Ca}_{0.75}\text{TiO}_3$	
	Theor.	Expt.	Theor.	Expt.	Theor.	Expt.	Theor.	Expt.
$a=b$	3.864	3.913	3.885	3.917	3.864	3.934	3.854	3.947
c	4.153	4.125	3.888	4.015	3.893	3.934	3.858	3.947
c/a	1.075	1.054	1.001	1.025	1.008	1.000	1.003	1.000
Ti	(0.500; 0.500; 0.539)		(0.500; 0.500; 0.539)		(0.500; 0.500; 0.500)		(0.500; 0.500; 0.500)	
O_{axial}	(0.500; 0.500; 0.111)		(0.500; 0.500; 0.103)		(0.500; 0.500; 0.106)		(0.50; 0.500; 0.106)	
$O_{\text{eq.}}$	(0.500; 0.000; 0.625)		(0.500; 0.000; 0.513)		(0.500; 0.000; 0.514)		(0.500; 0.000; 0.514)	

factor (c/a) decreases with increasing concentrations of Ca. Results described in the literature show that the best ferroelectric properties are around $x=0.25$ in $\text{Pb}_{1-x}\text{Ca}_x\text{TiO}_3$.^{8,9,15,16} Correlations between theoretical and experimental techniques can clarify this structural phase transition.

Theoretical-computational studies yield useful information regarding the electronic and structural properties of solids, which can provide a framework for the interpretation of experimental data in order to determine the influence of doping that often controls important aspects of solid-state chemistry. Periodic density functional theory (DFT) calculations provide detailed information regarding the properties of solid systems and serve as a fundamental tool for the interpretation of experimental data. Calculations based on the pseudopotential method with local-density approximation were correlated with results of XANES to elucidate hybridization among atoms in PCT and to identify their density of states (DOS) contributions.¹⁷ Fuks and co-workers developed a thermodynamic formalism based on the theoretical-computational approach of $\text{Ba}_c\text{Sr}_{(1-c)}\text{TiO}_3$ perovskite solid solution.¹⁸

Although ferroelectric and piezoelectric properties of perovskites have been extensively studied,¹⁹ few chemical bulk and surface properties of this material are described in the literature. Crystalline perovskite-type oxides show useful properties and are widely used as piezoelectric and ferroelectric materials. A prime example is the family of $\text{Pb}_{1-x}\text{Ca}_x\text{TiO}_3$ oxides, in particular, PbTiO_3 .²⁰⁻²²

Here is reported a theoretical and experimental study in which electronic properties are correlated with XRD and Raman results in relation to the phase transition induced by the increase in calcium concentration in $\text{Pb}_{1-x}\text{Ca}_x\text{TiO}_3$ solid solution, with $x=0.00, 0.25, 0.50$, and 0.75 .

This paper is organized as follows. Section II describes the experimental methods, spectral measurement techniques, the computing method, and model systems. Section III discusses the correlation between structural properties of XRD and DFT calculations, experimental Raman results and computational details. Section IV summarizes the main lines of our work.

II. METHODOLOGY

A. Experimental methods

$\text{Pb}_{1-x}\text{Ca}_x\text{TiO}_3$ powders were synthesized by the polymeric precursor method (PPM).²³⁻²⁷ In a transparent titanium cit-

rate solution prepared from titanium isopropoxide precursor (Riedel-de-Haën), stoichiometrically proportional amounts of calcium (first) and lead (second) acetate were added slowly to the solution under constant stirring and moderate heating until their complete dissolution. Ammonium hydroxide was used to prevent precipitation of lead citrate by adjusting the pH of the cations solution to around 6.0. In this homogeneous solution, ethylene glycol was added to promote the polyesterification reaction at 90°C .

After the water evaporated, the resin was heat-treated at 320°C for 2 hours in a static atmosphere, which led to the partial decomposition of the polymeric gel, forming an expanded resin composed of partially pyrolyzed material. The powders were then heat treated in a static air atmosphere at a heating rate of $10^\circ\text{C min}^{-1}$ in two heating steps. The first step was carried out at 350°C for 4 hours to pyrolyze the organic matter and the second one was carried out at 700°C for 2 hours to define the oxide crystalline structure.

Raman measurements were taken with a T-64000 Jobin-Yvon triple-monochromator attached to a charge coupled device (CCD) detector. An optical microscope with a $50\times$ objective lens was used to focus the 514.5 nm line of a Coherent Innova 90 argon laser onto the sample.

To evaluate the crystalline evolution and determine the unit cell parameters, we used a Rigaku DMax 2500 PC x-ray diffractometer with $\text{Cu } K_\alpha$ radiation ($\lambda=1.5406\text{ \AA}$) operating at room temperature. The data were collected in the $5^\circ-75^\circ$ 2θ range, with 0.006° step size by 10 s. A metallic Si internal standard was used to correct instrumental errors of the Bragg angle, and a Nelson-Riley extrapolation function was employed to evaluate the experimental lattice constants.⁶

B. Computing method and model systems

Periodic DFT calculations using Becke's three parameter hybrid nonlocal exchange functional²⁸ combined with the Lee-Yang-Parr gradient-corrected correlation functional,²⁹ B3LYP, were carried out by means of the CRYSTAL98 computer code.³⁰ We have been particularly successful in employing this function in studies of the electronic and structural properties of the bulk and surfaces of PbTiO_3 (Ref. 31) and BaTiO_3 (Ref. 32) systems. Pb, Ti, Ca, and O centers have been described in the scheme [DB]-31G, 86411-d(41), 86-511d3G, and 6-31G*, respectively. Here, [DB] stands for the Durand-Barthelat nonrelativistic large effective core

potential.³³ The basis sets can be found at the CRYSTAL home page.³⁴

As a first step, an optimization procedure of the lattice parameters was carried out, yielding values of $a=3.864$ Å and $c=4.153$ Å for the PbTiO₃ ($x=0.0$), space group $P4/mmm$ [see Table I and Fig. 1(a)]. Models representing Pb_{1-x}Ca_xTiO₃ at $x=0.25$, 0.50, and 0.75 were built within the supercell $2 \times 2 \times 1$ approach (Fig. 1) using tetragonal lattice constants. A supercell was obtained by defining the new translation vectors in terms of the old vectors. The total energy of all the models were minimized with respect to the tetragonal lattice constants and the z direction of the Ti and O internal atomic coordinates, using the Nelder-Mead minimization method.³⁵

The band structures were obtained at 80 k points along the appropriate high-symmetry paths of the adequate Brillouin zone. Diagrams of the density of states were built to analyze the corresponding electronic structures. The XCRYSDEN program³⁶ was used to draw the band structure diagram.

The theoretical DRX was obtained with the crystallographic software PCW (PowderCell) (Ref. 37) using the optimized lattice parameters and internal coordinates.

III. RESULTS

A. Correlation between structural properties of X-ray diffraction and density functional theory calculations

The theoretical and experimental XRD results of the lattice constants, atomic fractional coordinates, and tetragonality factor c/a for all models are summarized in Table I.

It is known that different concentrations of calcium in PbTiO₃ impose structural modifications (decrease of tetragonality), yielding a structure called pseudocubic. Several experimental works have demonstrated that tetragonality and unit cell volume decrease when calcium is added to the lead titanate lattice.^{19,38}

Our theoretical PbTiO₃ presents a large tetragonality factor, $c/a = 1.075$, in good agreement with the XRD experimental result, $c/a = 1.054$, at room temperature. Theoretical values from the PT tetragonal structure ($x=0.0$) to the pseudocubic structure ($x=0.25$, 0.50, and 0.75) show that the presence of Ca induces slight variations in the cell parameters, i.e., a decrease of the c parameter, leading to a small decrease of the tetragonality factor (Table I) as a function of the Ca concentration. XRD experimental results reveal the same behavior. Broadly, the theoretical results indicate that the tetragonal lattice tends toward a cubic symmetry. The distorted internal lattice parameters give us an asymmetric result of XRD for the pseudocubic structure. Such variations result from the tendency for progressive modifications in the lattice constants. The literature contains various descriptions of this behavior,^{8,9,15,19} which influences the Ca²⁺ ions in the modification of the lattice constants. The internal fractional coordinates show that the Ti atom is displaced in relation to the symmetric center of the perovskite unit cell. It is important to observe that, due to the displacement, the Ti atom and its six first neighbors do not form a center with an ideal cubic symmetry, e.g., PbTiO₃ with $Pm3m$ space group.

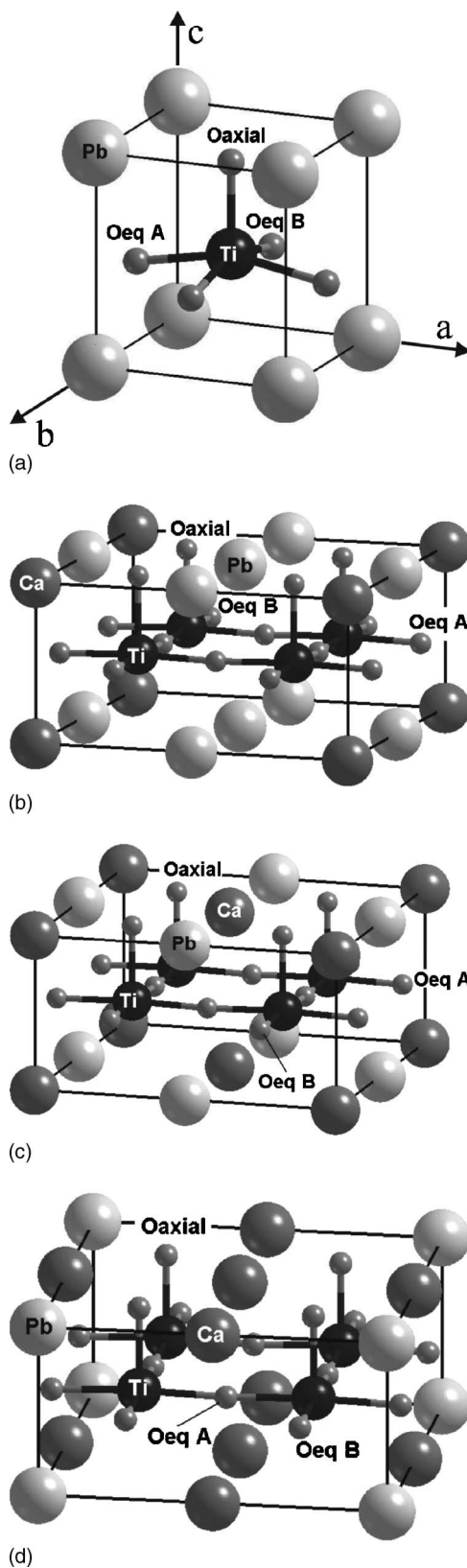


FIG. 1. Pb_{1-x}Ca_xTiO₃ cell structure: (a) $x=0.04$; (b) $x=0.25$; (c) $x=0.50$, and (d) $x=0.75$.

Similar experimental results were observed by Pontes *et al.*¹⁹ These authors reported an x-ray diffraction (XRD) analysis for several Ca contents. With $x=0.40$, the crystal

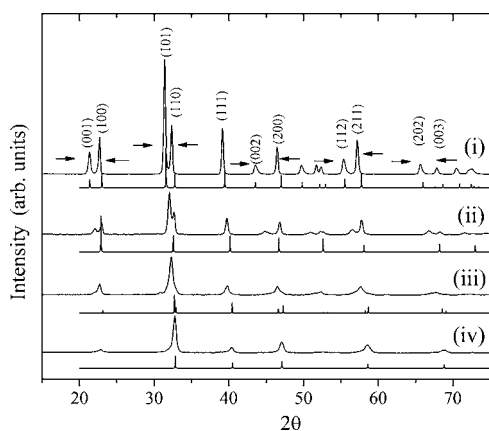


FIG. 2. Experimental (up) and theoretical (down) x-ray diffraction of $Pb_{1-x}Ca_xTiO_3$ solid system treated at $700\text{ }^\circ\text{C}$; (i) $x=0.0$, (ii) $x=0.25$, (iii) $x=0.50$, and (iv) $x=0.75$.

structure appeared as pseudocubic, while Raman scattering revealed a short tetragonality distortion. Some authors associate the decrease of tetragonality on $Pb_{1-x}Ca_xTiO_3$ solid solution to the increase of the calcium content up to nearly $x=0.40$ mole and, as a result of this addition, the perovskite system is arranged in an almost cubic structure (pseudocubic).

Analyzing the experimental x-ray diffraction (Fig. 2) of the powders treated at $700\text{ }^\circ\text{C}$, it is noted that these oxides are in a structural tetragonal perovskite arrangement. The XRD patterns of the PCT powders reveal some diffraction peak displacements in the $PbTiO_3$ phase, which reflect the variation in the interplanar distance of the (hkl) planes (001) and (100), (110) and (101), (002) and (200), (112) and (211), (202) and (003) owing to increased Ca doping.

These diffraction results are indexed according to tetragonal and cubic JCPDS cards Nos. 06-0452 ($P4/mm$) and 43-031 ($Pm3m$), respectively, indicating the formation of perovskite solid solution without the presence of secondary phases, which were undetectable by the XRD technique. The experimental results indicate that, with increasing amounts of calcium, the diffraction profiles show a tendency to form a cubic symmetry.

However, the theoretical XRD pattern of the 0.50 calcium amount in PCT solid solution shows several peaks relating to

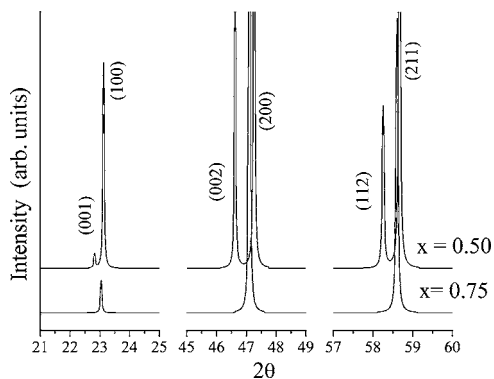


FIG. 3. Inset regions of theoretical x-ray diffraction for $x=0.50$ and $x=0.75$ PCT solid system.

TABLE II. Standard deviation (S) of lattice parameters a and c of the $Pb_{1-x}Ca_xTiO_3$ solid solution from the interplanar distance.

	Tetragonal			Cubic	
	PT	PCT _{0.25}	PCT _{0.50}	PCT _{0.75}	PCT _{0.75}
S_a	0.00435	0.00752	0.02669	0.02199	0.00905
S_c	0.00467	0.00922	0.01954	0.01612	0.00839

a tetragonal structure with a very low relative peak intensity. Figure 3 displays selected regions of theoretical diffractions for $x=0.50$ and 0.75 . The plane reflections presented in the 0.50 diffraction pattern of the theoretical data are not allowed in cubic $Pm3m$ symmetry. Initially, this affirmation is confirmed by comparing the cubic perovskite ICDD card No. 43-031 ($Pm3m$) diffraction with the experimental diffraction pattern in (iii) and (iv) of Fig. 2. Thus, for confirmation of the real long-range structure of PCT powders, the linear fitting of the interplanar distances to the equations of the cubic and tetragonal cells⁶ are compared in Table II. It is observed that for PCT $x=0.0$ and $x=0.25$, the XRD profiles are in agreement with the tetragonal cell, and the $x=0.50$ and 0.75 proportions show a smaller standard deviation from the cubic adjustment.

In principle, the x-ray technique is an excellent tool for the structural characterization of materials, but its major limitation is revealed in this system: No short range detection (internal coordinate).

In this section, we can make available the Vegard's law in relation to the atomic size and volume per valence electron in the structure. This effect shows the modification to a long range of the amount of calcium. We observe the decrease of the lattice constant c of linear form for theoretical and experimental results.

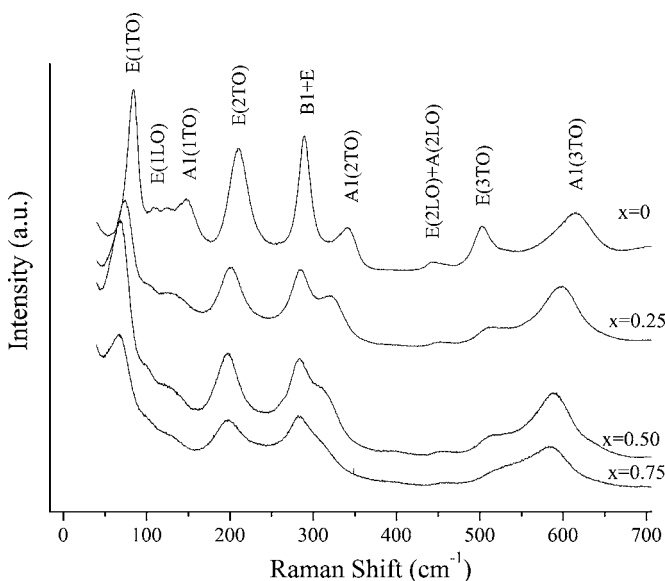


FIG. 4. Raman spectral dependence of the $Pb_{1-x}Ca_xTiO_3$ oxide system.

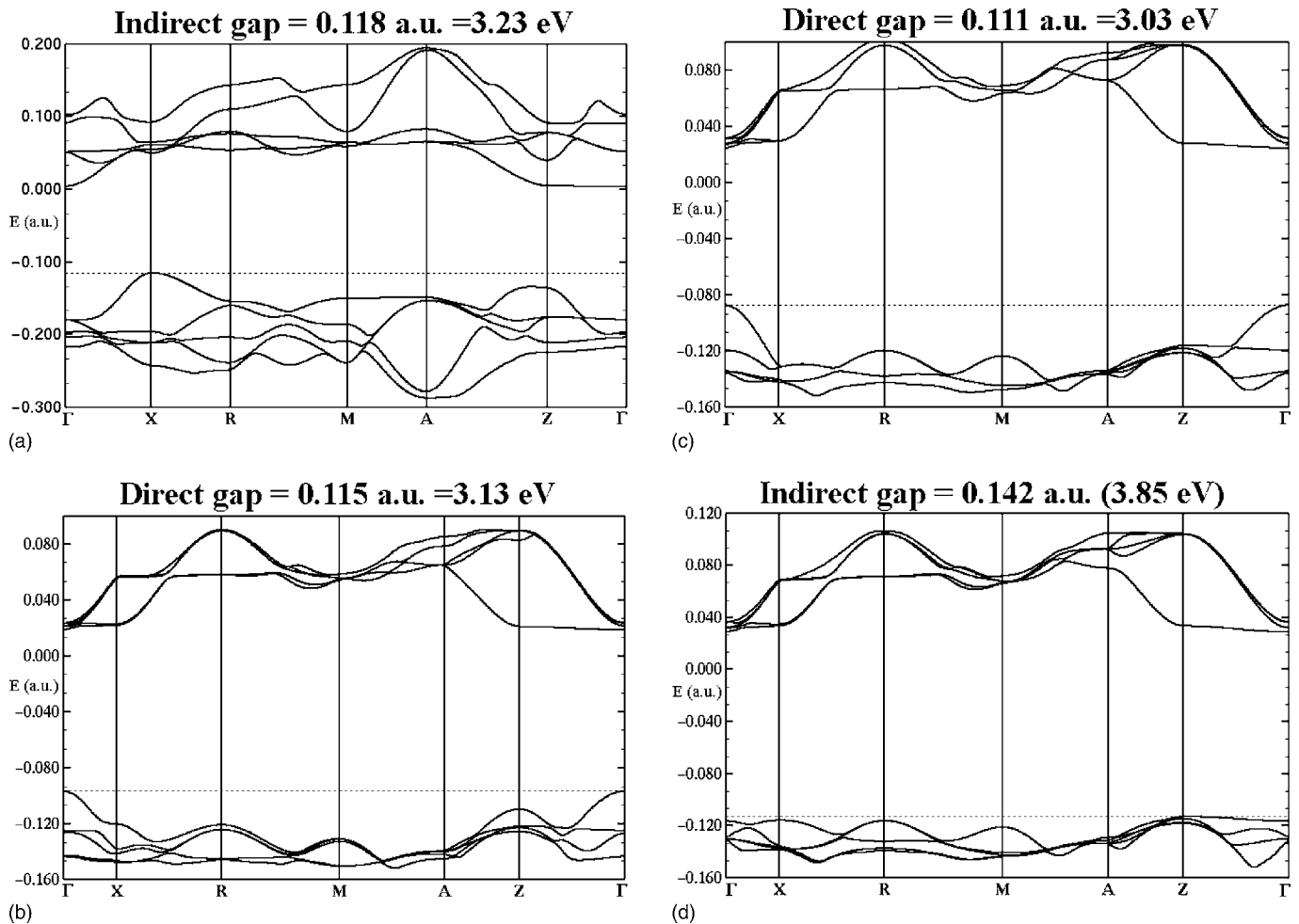


FIG. 5. Band structure of Pb_{1-x}Ca_xTiO₃ for (a) $x=0.0$, (b) $x=0.25$, (c) $x=0.50$, and (d) $x=0.75$.

B. Raman spectroscopy

In a previous statement, the theoretical and experimental results (Table I) indicated that the PbTiO₃ structure was tetragonal and the incorporation of calcium decreased the tetragonality factor c/a , leading the system to a nearly cubic structure, as demonstrated by the best fit of experimental data and calculated results (Table II).

According to Freire *et al.*,³⁹ $A_1(\text{TO})$ and $E(\text{TO})$ vibrational modes are associated with dipole moment displacements due to the vertical movement of oxygen and titanium in a direction parallel to the c lattice parameter. In tetragonal PbTiO₃, each T_{1u} mode splits into two vibrational modes in order to form A_1+E , while the T_{2u} mode splits into two modes in order to form B_1+E . All Raman and infrared modes are active in this symmetry group. However, in the cubic PbTiO₃ with O_{1h} symmetry, the 12 optical-phonon modes transform into the $3T_{1u}+T_{2u}$ irreducible representation. The T_{1u} modes are infrared active and the T_{2u} mode is silent, neither infrared nor Raman active. The T_{1u} modes are doubly degenerated in $T_{1u}(\text{TO})$ and $T_{1u}(\text{LO})$ modes (TO and LO are transverse and longitudinal to the k vector of polarizability, respectively).⁴⁰

The $E(1\text{TO})$ mode frequency, the soft mode, is the most sensitive to the decrease in the tetragonality factor of PCT, as

indicated in Fig. 4. However, for $x=0.50$ and $x=0.75$, the region where PCT would be cubic, where the Raman selection rules predict non-Raman active modes, the spectra clearly show several peaks. The presence of $E(1\text{LO})$, $E(2\text{TO})$, $E(2\text{LO})+A(2\text{LO})$, $E(3\text{TO})$ peaks can be attributed to local short-range disorder. An ideal cubic ABO₃ perovskite structure should not display any Raman-active modes in the first-order vibrational spectrum. However, lowering the symmetry leads to changes in vibrational spectra and selection rules, so that first-order Raman scattering is then allowed.⁴¹⁻⁴³

From the Raman spectra (Fig. 4), it is clear that the structure does not belong to a tetragonal-cubic transition, but to an increasing symmetry with the conservation of a short-range disorder.

C. Band structures and density of states (DOS)

Figure 5 shows the band structure for $x=0.0$, 0.25, 0.50, and 0.75. There is a slight variation in the band gap with the increase in Ca concentration. For $x=0.0$ (PT), our theoretical results indicate an indirect band gap [Fig. 5(a)], 3.23 eV, between X and Γ points.^{44,45}

When $x=0.25$, the top of the valence band is displaced from the X point of the Brillouin zone to the Γ point. Thus,

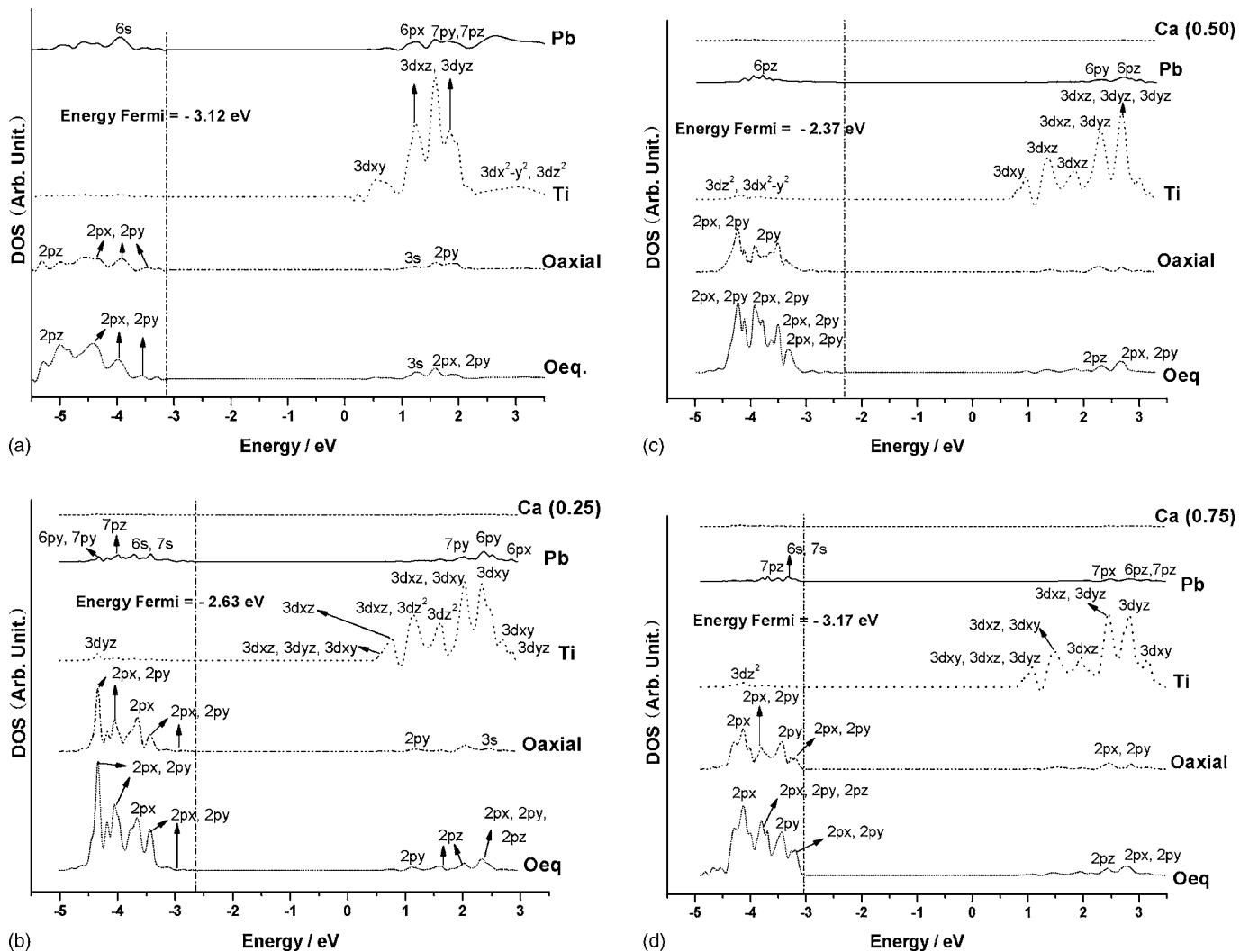


FIG. 6. Density of states profiles for Ca, Pb, Ti, O_{axial} and O_{eq} atoms in the $Pb_{1-x}Ca_xTiO_3$ solid solution.

the optical band gap, 3.13 eV [Fig. 5(b)], becomes direct at the Γ point. The lowest conduction band (CB) is flat between the Γ -X and Z- Γ points. The shape between Z and Γ points is very similar to the PT case. For $x=0.50$ [Fig. 5(c)], the band gap is direct, 3.03 eV, at the Γ point. The CB profile is similar to $x=0.25$. When $x=0.75$ [Fig. 5(d)], the top of valence band (VB) is located at the Z point, and the gap again becomes indirect, 3.85 eV, between the Z and Γ points. The top of the upper valence band at the Γ , X, and R points comes out around 0.1 eV below the highest state at the Z point. Again, the lowest CB between Γ -X and Z- Γ points are flat. For $x=0, 0.25$, and 0.50 there is a lower variation in the gap of the oxides; however, at $x=0.75$ there is an increase of this value due to the increase of the amount of Ca. This behavior can be a correlation to the existence of a particular molecular structure where the bands are reorganized in relation to $PbTiO_3$ bands, but the gap is not significantly modified. The band structures demonstrated the Brillouin-zone effects of Vegard's law. There is a correspondence among bands and the increase of the amount of calcium. It was observed that at the top of the VB there is a change of X point ($PbTiO_3$) and Γ and Z points (PCT); this is the influence on the short range of the Vegard's law.

The density of states in different calcium contents is summarized in Fig. 6. The major atomic orbital (AO) of the selected bands was analyzed with a threshold of 0.15 for the eigenvector coefficients.

In calcium concentration of $x=0.25, 0.50$, and 0.75, it can be observed that Ca atoms do not contribute in the -5 eV to 3.5 eV energy range; however, this contribution is located in another energy range.¹⁷ For $PbTiO_3$ [Fig. 6(a)], the analysis of the atomic orbitals (AOs) contributions to the top of VB shows mainly derived $2p_x$ and $2p_y$ orbitals of O atoms. $PbTiO_3$ CB is constituted mainly of Ti 3d orbitals.

For $Pb_{0.75}Ca_{0.25}TiO_3$, the VB is constituted of the 2p states of O atoms and display the lowest contributions of the Ti $3d_{yz}$ state at nearly -4.5 eV [Fig. 6(b)]. The Pb 7s, 6s, and 7p levels are found between -3.5 and -4.5 eV. The main contribution of the CB in this calcium concentration comes from the Ti 3d character.

The calcium content of $x=0.50$ mol [Fig. 6(c)] shows the same behavior as $x=0.25$, with a lower decrease in the O_{eq} (see Fig. 1) 2p states character. When $x=0.75$, the contributions of O_{axial} and O_{eq} 2p states are displaced to Fermi energy value [Fig. 6(d)]. The Pb states present the same behavior. The main contribution to the CB of $Pb_{0.25}Ca_{0.75}TiO_3$

TABLE III. Mulliken charges (in $|e|$) of the atoms in Pb_{1-x}Ca_xTiO₃ unit cells.

	PT	PCT _{0.25}	PCT _{0.50}	PCT _{0.75}
Ti	2.175	2.184	2.177	2.171
Pb	1.021	1.065	1.063	1.072
Ca		1.593	1.595	1.587
O _{axial}	-1.002	-1.123	-1.172	-1.206
O _{eq,a}	-1.097	-1.087	-1.167	-1.170
O _{eq,b}		-1.169		-1.250
TiO ₆	-0.520	-0.637	-0.770	-0.846

solid solution again comes from Ti 3*d* levels.

Overall, Pb atoms do not play a preponderant role in the modification of states with the increase of calcium concentration in the solid solution. The Ca AOs do not contribute directly to the gap energy range; however, the shape of O, Ti, and Pb AOs are influenced by the calcium substitution. The contributions of Ti and O atoms between -2.5 and -5.0 eV are characterized as hybridizations between the 3*d* and 2*p* AOs of these atoms.⁴⁶ For the oxygen atoms, the excessive contributions in the VB are interactions mentioned as nonbonding states where the electrons are located. For the Ti atoms, the excessive contributions to the CB are nonbonding states where the holes are located.

With the presence of Ca atoms in solid solution, titanium 3*d* states oriented in the *z* direction are redistributed to lower energy states.

The DOS results indicates that even though calcium states do not contribute to the band gap and the Pb states DOS profiles hardly change at all, the Ti 3*d* and O 2*p* states in Pb_{1-x}Ca_xTiO₃ are perturbed with increased calcium concentrations. This perturbation of Ti 3*d* and O 2*p* states is responsible for the phase transition and increased long-range structural symmetry.

D. Mulliken charges

The atomic charges obtained from Mulliken analysis of all the models are presented in Table III. The choice of the Mulliken partition is arbitrary, since there is no single method for partitioning the charge density. However, the choice of the given scheme is still extremely useful for comparing the tendencies revealed in the results of the calculations using similar models.⁴⁷ As can be seen in this table, an increase in the amount of Ca increased the positive charge of the Pb atoms. However, the charge of the Ti atom was not significantly modified. The O_{axial} (see Fig. 1) showed an increase in the negative charge with increasing amounts of calcium. This behavior is due to fact that the O_{axial} is responsible for the simultaneous interactions between Pb-O and Ca-O. This indicates that, as the amount of calcium increases, so does the positive charge of the Pb atoms and the negative charge in the O_{axial} atoms. The difference in charges among the oxygen atoms (Table III)—O_{eqA}, O_{eqB}, and O_{axial}—may be responsible for the distinct ferroelectric and piezoelectric properties due to the influence on the Ca and Pb

TABLE IV. Overlap populations (in $m|e|$) to Ti-O, Pb-O, and Ca-O bonds.

	PT	PCT _{0.25}	PCT _{0.50}	PCT _{0.75}
Ti-O	62	58	56	54
Pb-O	20	16	8	9
Ca-O		19	18	20

atoms when $x=0.25$ and $x=0.75$. In such cases, the negative charge in both atoms increases, indicating that these atoms are not equivalent to those in the proportions of $x=0.0$ and 0.50. Therefore, the number of different neighbors, Pb²⁺ and Ca²⁺ ions, yield the formation of an asymmetric center of charges among the various proportions. This asymmetric center of charges occurs because of unequal electron density due to different bonds yielding a heterogeneous interaction field. Such an effect causes an irregularity in the lattice constants and the internal coordinate.

The calculations of the electronic structure also give us access to the charge repartition inside the unit cell, for instance the TiO₆ cluster. These cluster charges show the influence of the neighboring atoms, Pb and Ca, in relation to the Ti atom. An increase of negative charge in the TiO₆ cluster is observed when the amount of Ca increases (Table III), deforming the electronic structure and modifying the Ti-O interaction. This interaction is very important for the piezoelectric and ferroelectric effect.⁴⁸

E. Overlap population

The overlap population is a measure of the shared electronic density between two atomic nucleus. This result expresses that the kind of interaction between atoms conforms to modifications in the crystalline structure. With the decrease of overlap population, the covalent interaction decreases, showing an ionic bond nature. However, the increase of overlap population suggests the improvement of electronic density sharing between atoms, enhancing the covalent interaction on the oxide bonds. The total overlap population for any pair of atoms is in general made up of positive (bonding) and negative (antibonding) contributions.⁴⁹ A simple way to know the bonds characteristics in ceramic oxides, is analyzing the cation-oxygen interaction. The overlap population results as a function of different calcium concentrations in PbTiO₃ are presented in Table IV.

Note that the overlap population in the Ti-O and Pb-O bonds decreases and the Ca-O have slight variation. The influence of the quantity of Ca is localized in the displacement of the electronic density from Ti-O and Pb-O bonds. In other words, the Pb for Ca substitution in PbTiO₃ host lattice increases the ionic nature of PCT solid solution.

The relationship of electronegativity between Pb and Ca atoms in these results is evident. Electronegativity of these elements is evidenced by the difference in the overlap population of the Pb atom on the undoped and doped PbTiO₃ host lattice.

IV. SUMMARY

Theoretical and experimental studies of the solid solution pseudocubic phase of Pb_{1-x}Ca_xTiO₃, a product of the substi-

tution of Pb^{2+} ions for Ca^{2+} ions in the PbTiO_3 lattice, were conducted employing both XRD and Raman results and periodic first-principles calculations based on the B3LYP functional. The main conclusions of this work can be summarized as follows:

(i) The bulk equilibrium geometries are in agreement with the experimental results. The structures have a tendency to change from the tetragonal group to the cubic group, whereas the internal coordinates of the Ti atom and its first six neighbors do not form an ideal symmetrical cubic arrangement. The XRD and Raman results corroborate the theoretical analysis. The pseudocubic phase shows characteristics of tetragonal and cubic groups.

(ii) The calculated optical band gaps are 3.23, 3.13, 3.03, and 3.85 eV for $x=0.0$, 0.25, 0.50, and 0.75, respectively. Splitting of the Fermi energy occurs, and the gap is indirect for $x=0.0$ and 0.75 and direct for $x=0.25$ and 0.50. The z direction of the Ti $3d$ states stabilizes with the presence of Ca.

(iii) Pb^{+2} and Ca^{+2} ions modify the Mulliken charges of O_{ax} and O_{eq} . This effect influences the lattice constants and

internal coordinates. These results suggest that the quantity of Ca in PT for $x=0.25$ and $x=0.75$ modifies the material's polarizability, which is responsible for the ferroelectricity.

(iv) Increasing the amount of calcium augments the ionic character of the Ti-O, especially in the Pb-O interactions, as indicated by the decrease in the overlap population in the Ti-O and Pb-O bonds.

(v) It is possible to verify the Vegard's law in long range (XDR) and short range (band structure and overlap population). Such law presents macroscopic and microscopic factors for explanation of the lattice contraction in alloys or solid solutions.

ACKNOWLEDGMENTS

This work was supported by the Brazilian research funding agencies FAPESP, CAPES, CNPq and by the Fundació Caixa Castelló-Bancaixa, Spain. The use of the computer facilities of the Servei d'Informàtica (Universitat Jaume I) and Laboratório de Simulação Molecular, Unesp, Bauru, are also gratefully acknowledged.

*Laboratório Interdisciplinar de Eletroquímica e Cerâmica; url: <http://www.liec.ufscar.br/ceramica>; Electronic address: sergio@lieg.ufscar.br

¹Z.-X. Chen, Y. nChen, and Y.-S. Jiang, *J. Phys. Chem. B* **106**, 9986 (2002).

²M. E. Lines and A. Glass, *Principles and Application of Ferroelectrics and Related Materials* (Clarendon, Oxford, 1977).

³J. F. Scott, *Phys. World* **8**, 46 (1995).

⁴Y. K. Tseng, K. S. Liu, J. D. Jiang, and I. N. Lin, *Appl. Phys. Lett.* **72**, 3285 (1998).

⁵A. I. Frenkel, D. M. Pease, J. Giniewicz, E. A. Stern, D. L. Brewre, M. Daniel, and J. Budnick, *Phys. Rev. B* **70**, 014106 (2004).

⁶C. Suryanarayana and M. G. Norton, *X-Ray Diffraction: A Practical Approach* (Plenum, New York, 1998).

⁷X. G. Tang, H. L. W. Chan, and A. L. Ding, *Solid State Commun.* **127**, 625 (2003).

⁸D. H. Bao, X. Q. Wu, L. Y. Zhang, and X. Yao, *Thin Solid Films* **350**, 30 (1999).

⁹V. V. Lemanov, A. V. Sotnikov, E. P. Smirnova, and M. Weihnacht, *Appl. Phys. Lett.* **81**, 886 (2002).

¹⁰A. Chandra and D. Pandey, *J. Mater. Res.* **18**, 407 (2003).

¹¹L. Vegard, *Z. Phys.* **5**, 17 (1921).

¹²A. R. Denton and N. W. Ashcroft, *Phys. Rev. A* **43**, 3161 (1991).

¹³H. Axon and W. Hume-Rothery, *Proc. R. Soc. London, Ser. A* **193**, 1 (1948).

¹⁴F. M. Pontes, D. S. L. Pontes, E. R. Leite, E. Longo, A. J. Chiquito, M. A. C. Machado, P. S. Pizani, and J. A. Varela, *Appl. Phys. A: Mater. Sci. Process.* **78**, 349 (2004).

¹⁵S. Chopra, S. Sharma, T. C. Goel, and R. G. Mendiratta, *Solid State Commun.* **127**, 299 (2003).

¹⁶J. Mendiola, P. Ramos, and M. L. Calzada, *J. Phys. Chem. Solids* **59**, 1571 (1998).

¹⁷J. C. Jan, K. P. K. Kumar, J. W. Chiou, H. M. Tsai, H. L. Shih, H. C. Hsueh, S. C. Ray, K. Asokan, W. F. Pong, M. H. Tsai *et al.*, *Appl. Phys. Lett.* **83**, 3311 (2003).

¹⁸D. Fuks, S. Dorfman, S. Piskunov, and E. A. Kotomin, *Phys. Rev. B* **71**, 014111 (2005).

¹⁹F. M. Pontes, D. S. L. Pontes, E. R. Leite, E. Longo, E. M. S. Santos, S. Mergulhao, A. Chiquito, P. S. Pizani, F. Lanciotti, T. M. Boschi *et al.*, *J. Appl. Phys.* **91**, 6650 (2002).

²⁰G. Borstel, R. I. Eglitis, E. A. Kotomin, and E. Heifets, *J. Cryst. Growth* **237**, 687 (2002).

²¹K. van Benthem, C. Elsasser, and R. H. French, *J. Appl. Phys.* **90**, 6156 (2001).

²²S. Piskunov, E. Heifets, R. I. Eglitis, and G. Borstel, *Comput. Mater. Sci.* **29**, 165 (2004).

²³P. R. de Lucena, O. D. Pessoa-Neto, I. M. G. dos Santos, A. G. Souza, E. Longo, and J. A. Varela, *J. Alloys Compd.* **397**, 255 (2005).

²⁴E. Leite, C. Sousa, E. Longo, and J. Varela, *Ceram. Int.* **21**, 143 (1995).

²⁵M. Kakihana, *J. Sol-Gel Sci. Technol.* **6**, 7 (1996).

²⁶D. S. L. Pontes, E. R. Leite, F. M. Pontes, E. Longo, and J. A. Varela, *J. Mater. Sci.* **36**, 3461 (2001).

²⁷P. R. de Lucena, E. R. Leite, F. M. Pontes, E. Longo, P. S. Pizani, and J. A. Varela, *J. Solid State Chem.* **179**, 3997 (2006).

²⁸A. D. Becke, *J. Chem. Phys.* **98**, 5648 (1993).

²⁹C. T. Lee, W. T. Yang, and R. G. Parr, *Phys. Rev. B* **37**, 785 (1988).

³⁰R. Dovesi, V. R. Saunders, and C. Roetti, *CRYSTAL98 User's Manual* (University of Torino, Torino, 1998).

³¹S. de Lázaro, E. Longo, J. R. Sambrano, and A. Beltrán, *Surf. Sci.* **552**, 149 (2004).

³²J. R. Sambrano, E. Orhan, M. F. C. Gurgel, A. B. Campos, M. S. Goes, C. O. Paiva-Santos, J. A. Varela, and E. Longo, *Chem.*

- Phys. Lett. **402**, 491 (2005).
- ³³P. Durand and J. C. Barthelat, *Theor. Chim. Acta* **38**, 283 (1975).
- ³⁴CRYSTAL98, www.crystal.unito.it/
- ³⁵J. A. Nelder and R. Mead, *Comput. J.* **7**, 308 (1965).
- ³⁶A. Kokalj, *J. Mol. Graphics Modell.* **17**, 176 (1999).
- ³⁷W. Kraus and G. Nolze, *J. Appl. Crystallogr.* **29**, 301 (1996).
- ³⁸A. L. Kholkin, I. Bdikin, Y. I. Yuzyuk, A. Almeida, M. R. Chaves, M. L. Calzada, and J. Mendiola, *J. Cryst. Growth* **85**, 176 (2004).
- ³⁹J. D. Freire and R. S. Katiyar, *Phys. Rev. B* **37**, 2074 (1988).
- ⁴⁰G. Burns and B. A. Scott, *Phys. Rev. B* **7**, 3088 (1973).
- ⁴¹S.-Y. Kuo, C.-T. Li, and W.-F. Hsieh, *Phys. Rev. B* **69**, 184104 (2004).
- ⁴²J. Rouquette, J. Haines, V. Bornand, M. Pintard, P. Papet, R. Astier, J. M. Léger, and F. Gorelli, *Phys. Rev. B* **65**, 214102 (2002).
- ⁴³H. Zheng, I. M. Reaney, and G. D. C. C. de Györgyfalva, *J. Mater. Res.* **19**, 488 (2004).
- ⁴⁴E. R. Leite, L. P. S. Santos, N. L. V. Carreno, E. Longo, C. A. Paskocimas, J. A. Varela, F. Lanciotti, C. E. M. Campos, and P. S. Pizani, *Appl. Phys. Lett.* **78**, 2148 (2001).
- ⁴⁵Q. Zhao, Z. X. Fan, Z. S. Tang, X. J. Meng, J. L. Song, G. S. Wang, and J. H. Chu, *Surf. Coat. Technol.* **160**, 173 (2002).
- ⁴⁶E. Orhan, F. M. Pontes, M. A. Santos, E. R. Leite, A. Beltran, J. Andres, T. M. Boschi, P. S. Pizani, J. A. Varela, C. A. Taft *et al.*, *J. Phys. Chem. B* **108**, 9221 (2004).
- ⁴⁷C. Pisani, R. Dovesi, and C. Roetti, *Hartree-Fock Ab Initio Treatments of Crystalline Systems* (Springer-Verlag, Berlin, 1988).
- ⁴⁸R. E. Cohen, *Nature (London)* **358**, 136 (1997).
- ⁴⁹R. S. Mulliken, *J. Chem. Phys.* **23**, 1833 (1955).